

Insights into the physical properties and anisotropic nature of ErPdBi with an appearance of low minimum thermal conductivity

S K Mitro, R Majumder, K M Hossain, Md Zahid Hasan, Md Emran Hossain, and M A Hadi

Citation: Chin. Phys. B, 2021, 30 (**1**): 016203. DOI: 10.1088/1674-1056/abaf9d
Journal homepage: http://cpb.iphy.ac.cn; http://iopscience.iop.org/cpb

What follows is a list of articles you may be interested in

Plastic deformation mechanism transition of Ti/Ni nanolaminate with pre-existing crack: Molecular dynamics study

Meng-Jia Su(宿梦嘉), Qiong Deng(邓琼), Min-Rong An(安敏荣), Lan-Ting Liu(刘兰亭)
Chin. Phys. B, 2020, 29 (**11**): 116201. DOI: 10.1088/1674-1056/aba2e5

Improvement of high-frequency properties of Co_2FeSi Heusler films by ultrathin Ru underlayer

Cuiling Wang(王翠玲), Shouheng Zhang(张守珩), Shandong Li(李山东), Honglei Du(杜洪磊), Guoxia Zhao(赵国霞), Derang Cao(曹德让)
Chin. Phys. B, 2020, 29 (**4**): 046202. DOI: 10.1088/1674-1056/ab7802

Anisotropic plasticity of nanocrystalline Ti: A molecular dynamics simulation

Minrong An(安敏荣), Mengjia Su(宿梦嘉), Qiong Deng(邓琼), Haiyang Song(宋海洋), Chen Wang(王晨), Yu Shang(尚玉)
Chin. Phys. B, 2020, 29 (**4**): 046201. DOI: 10.1088/1674-1056/ab7188

Orientation dependence of elastic properties in orthorhombic $Ca_3Mn_2O_7$

Gang Jian(简刚), Mei-Rui Liu(刘美瑞), Chen Zhang(张晨), Jie Lu(卢杰), Chao Yan(晏超)
Chin. Phys. B, 2019, 28 (**2**): 026201. DOI: 10.1088/1674-1056/28/2/026201

Anisotropy of elasticity and minimum thermal conductivity of monocrystal M_4AlC_3 (M=Ti, Zr, Hf)

Ding Ai-Ling, Li Chun-Mei, Wang Jin, Ao Jing, Li Feng, Chen Zhi-Qian
Chin. Phys. B, 2014, 23 (**9**): 096201. DOI: 10.1088/1674-1056/23/9/096201

Insights into the physical properties and anisotropic nature of ErPdBi with an appearance of low minimum thermal conductivity

S K Mitro[1], R Majumder[2,†], K M Hossain[3], Md Zahid Hasan[4], Md Emran Hossain[2], and M A Hadi[5]

[1] *Bangamata Sheikh Fojilatunnesa Mujib Science and Technology University, Jamalpur-2012, Bangladesh*
[2] *Physics Discipline, Khulna University, Khulna-9208, Bangladesh*
[3] *Department of Materials Science and Engineering, University of Rajshahi, Rajshahi-6205, Bangladesh*
[4] *Department of Electrical and Electronic Engineering, International Islamic University Chittagong, Kumira, Chittagong-4318, Bangladesh*
[5] *Department of Physics, University of Rajshahi, Rajshahi, 6205, Bangladesh*

(Received 24 June 2020; revised manuscript received 12 August 2020; accepted manuscript online 15 August 2020)

We theoretically study the structural, elastic and optical properties of ErPdBi together with its anisotropic behaviors using density functional theory. It is observed that ErPdBi satisfies the Born stability criteria nicely and possesses high quality of machinability. The anisotropic behavior of ErPdBi is reported with the help of theoretical anisotropy indices incorporating 3D graphical presentation, which suggests that ErPdBi is highly anisotropic in nature. It is noticed that the minimum thermal conductivity is very low for ErPdBi compared to the several species. This low value of minimum thermal conductivity introduces the potentiality of ErPdBi in high-temperature applications such as thermal barrier coatings. In addition, deep optical insights of ErPdBi reveal that our material can be used in different optoelectronic and electronic device applications ranging from organic light-emitting diodes, solar panel efficiency, waveguides etc. to integration of integrated circuits. Therefore, we believe that our results will provide a new insight into high-temperature applications and will benefit for the development of promising optoelectric devices as well.

Keywords: ErPdBi, minimum thermal conductivity, anisotropy, density functional theory (DFT)

PACS: 62.20.Dc, 78.20.Ci, 31.15.E– **DOI:** 10.1088/1674-1056/abaf9d

1. Introduction

Recently, ternary half-Heusler (THH) compounds are drawing more attention from the research community for their interesting properties such as heavy Fermionic behavior,[1] giant magnetoresitivity,[2] superconductivity[3] and thermoelectricity.[4,5] Their flexible band gap with tuning ability ranging from wide band gap semiconductor to zero band gap insulator make them the "properties on request".[1–6] They possess very simple structures with a tunable 1:1:1 formulation composed of XYZ (X and Y represent transition metal (TM) elements and Z implies sp atoms). Among these THHs, some Pd-based THHs are becoming very significant due to their exposure of new topological quantum state, namely topological insulator and excellent features of ultrahigh mobility.[7] They possess very high thermoelectric power factors near room temperature together with linear dispersion and quantum magnetoresistance.[7–9] Among these Pd-based THHs, ErPdBi has been investigated extensively in some experimental literature considering its possible potentiality in several dimensions.[10–13] Pavlosiuk *et al*. studied the magnetic order and Shubnikovde–Haas oscillations. Pan *et al*.[10,11] reported superconducting features with magnetic order. Sekimoto *et al*.[12] reported thermoelectric and thermophysical behaviors of ErPdBi and concluded that ErPdBi possesses positive thermoelectric power which is very important for several thermoelectric applications. Again, Pavlosiuk *et al*.[13] reported the magnetic structure of our studied material. While there have been some studies on ErPdBi, no theoretical study is available yet and more information on this compound needs to be disclosed for understanding this system perfectly. In view of materials science, elastic properties are a remarkable parameter linked with several physical behaviors of a material system. The mechanical and elastic stability is an important factor which measures the ability and suitability of a material for device fabrications and applications. The material systems which reveal well mechanical stability and machinability are always easy to handle for different purposes. At the same time, deep optical analysis of a material gives the information about the interaction of materials with incident photons, and the information is very much effective for optoelectronic, dielectric applications ranging from solar cells, solar photovoltaics, waveguides, solar cell coating, light-emitting diodes (LEDs), organic light-emitting diodes (OLEDs) to large scale integration of integrated circuits.[14–17] Therefore, the primary objective of this work is to investigate the elastic and optical properties of ErPdBi for proper exploration of mechanical stability and inquiry into the flexibility of device fabrication under different external conditions of the material under study, as well as to justify the suitability of optoelectronic applications by detailed optical analysis. On the other hand, possibilities of cracking, lattice distortion and plastic deformation can be evaluated successfully by studying the anisotropic features of

†Corresponding author. E-mail: rinkumajumder02@gmail.com

© 2021 Chinese Physical Society and IOP Publishing Ltd

a material.[17] Proper investigation of anisotropy enables us to improve the mechanical quality as well as ability of materials performance under external pressure and temperature, which is basically important in crystal science engineering and industrial aspects.[17] Equally important, low minimum thermal conductivity of a material is another important factor in high temperature applications such as thermal barrier coating and solid-state refrigerators.[14,17] To the best of our knowledge, both anisotropic nature and minimum thermal conductivity of ErPdBi have not been calculated yet. Therefore, the main purpose of this research is to investigate the anisotropic nature as well as the minimum thermal conductivity (κ_{min}) of ErPdBi.

2. Method of calculations

The present study was designed for the investigation of structural, mechanical, electronic, and thermodynamic behavior of ErPdBi by exploiting the most commonly used computer program CASTEP (Cambridge Serial Total Energy Package)[18] in the frame of density functional theory (DFT).[19,20] The exchange-correlation function of generalized gradient approximation (GGA) associated with Perdew–Burke–Ernzerhof (PBE)[21] have been executed for this calculation. The well-known norm-conserving pseudopotential[22] was treated to consider the interaction among valance electrons and ions for all atoms. For ErPdBi, the valence electron orbital $4d^{12}$ for palladium (atomic No. 46), $4f^{12}6s^2$ for erbium (atomic No. 68) and the $6s^2\ 6p^3\ 5d^{10}$ for bismuth (atomic No. 83) were chosen. In the case of structural analysis, both ultrasoft Vanderbilt-type pseudopotentials and norm-conserving pseudopotential have been used to compare our results. Otherwise, in all types of calculations, we have considered the norm-conserving pseudopotential to describe the interaction among the valence electrons with ions, nuclei and the core electrons for Er, Pd, and Bi atoms.[22] Since the constituents of this material involve mass number greater than 50, for all types of calculations we have included spin orbit interaction.[23] To ascertain well convergence of the calculated geometrical optimization and the elastic constant, cut-off energy of plane wave was used at 600 eV and the k-point mesh of $9 \times 9 \times 9$ grids was selected to sample the Monkhorst–Pack scheme[24] for the ErPdBi system. The structure has been optimized with the help of the Broyden–Fletcher–Goldferb–Shanno (BFGS) algorithm.[25] The unit cell and atomic relaxation have been executed considering the total energy 5×10^{-6} eV/atom, maximum force 0.01 eV/Å, maximum stress 0.02 GPa and maximum ionic displacement 5×10^{-4} Å.

The elastic constants and moduli have been obtained by employing a set of finite homogeneous crystal deformations as implemented in the CASTEP code, based on the stress-strain method.[26] The energy-dependent (frequency dependent) optical properties of the compound have been evicted from the complex dielectric function which describes the interactions of photons with electrons, expressed by $\varepsilon(\omega) = \varepsilon_1(\omega) + i\varepsilon_2(\omega)$. The imaginary part of the complex dielectric function, $\varepsilon_2(\omega)$, can be calculated with the help of the CASTEP code incorporated with the transition probabilities between occupied and unoccupied orbital electronic states by the following equation:[15]

$$\varepsilon_2(\omega) = \frac{2\pi e^2}{\Omega \varepsilon_0} \sum_{k,v,c} |\langle \psi_k^c | \hat{u}.r | \psi_k^v \rangle|^2 \delta(E_k^c - E_k^v - \hbar\omega). \quad (1)$$

Here the delta function δ ensures the conservation of energy and momentum during the optical transition while e, Ω, ψ_k^c, and ψ_k^v represents the electronic charge, unit cell volume, conduction band and valence band wave functions at a given wave-vector k, respectively; and $\hat{u}$ is the vector defining the electric field polarization of the incident light. Using the Kramers–Kronig transformations, one can easily find the real part of dielectric function from the corresponding imaginary part ε_2 (ω). Once the two basic parameters $\varepsilon_1(\omega)$ and $\varepsilon_2(\omega)$ are known, other optical parameters, $n(\omega)$, $k(\omega)$, $\sigma(\omega)$, $\alpha(\omega)$, $R(\omega)$ and$L(\omega)$, can be obtained from them.[27]

3. Results and discussion

3.1. Structural and electronic properties

The structure of THH ErPdBi has been constructed by considering the Bi at 4*a* (0, 0, 0), Er at 4*b* (1/2, 1/2, 1/2) and Pd at 4*c* (1/4, 1/4, 1/4) in the unit cell.[14,17] The optimized conventional unit cell (2D view and 3D view) of ErPdBi has been shown in Fig. 1, and both the views possess the cubic MgAgAs-type crystal structure with the $F\bar{4}3m$ space group like other THHs.[14,17] We have determined the ground state structural properties such as lattice constants a and unit cell volume V_0 by minimizing the total energy and force convergence at zero pressure and temperature. The equilibrium lattice parameters and unit cell volumes obtained in this study have been listed in Table 1. We have used two pseudopotential optimization schemes GGA-OTFG ultrasoft and GGA-Norm conserving to be confirmed for the further analysis ensuring better accuracy. The obtained optimized lattice constants from GGA-OTFG ultrasoft and GGA-Norm conserving pseudopotential were 6.810 Å and 6.621 Å, respectively. Between these two observed lattice constants obtained from two different pseudopotentials, the lattice constants from GGA-Norm conserving approach are more consistent with the experimental data, which testifies the credibility and accuracy of our calculations.[10,11] There is no theoretical data available yet to compare our results. It can be observed that lattice constants obtained from GGA-Norm conserving method are less (close to the published experimental data) than those obtained from the GGA-OTFG ultrasoft method. Therefore for further analysis we have used norm-conserving pseudopotential. It is worth mentioning that norm conserving pseudopotential is preferred than ultrasoft pseoudo potential to include the spin orbit interaction properly and for the calculation of structural, electronic, elastic and optical properties preciously.[14,28,29]

Table 1. Unit cell parameters and cell volume of cubic ErPdBi in contrast to experimental data.

Compound	Calculated (GGA-OTFG ultrasoft)		Calculated (GGA-Norm conserving)		Expt.[10,11]	
	a (Å)	V_0 (Å^3)	a (Å)	V_0 (Å^3)	a (Å)	V_0 (Å^3)
ErPdBi	6.810	315.82	6.621	290.25	6.589[10]	286.06*
					6.595[11]	286.84*

*Calculated by us using published experimental lattice constants a.

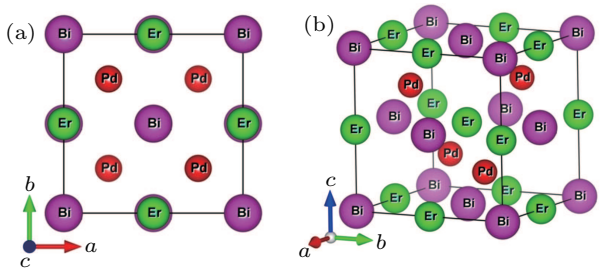


Fig. 1. Conventional unit cell of ErPdBi: (a) 2D view in xy plane, (b) 3D view in xyz directions.

The electronic band structure (BS) of THH compound ErPdBi in cubic phase with equilibrium lattice constant calculated along the high symmetry points at W (1/4, 3/4, 1/2), L (1/2, 1/2, 1/2), Γ (0, 0, 0) and X (0, 1, 1) is shown in Fig. 2. The horizontal dotted line is set at zero of energy scale defined as the Fermi level E_F. The overall nature of the calculated BS is the same as those reported for several Bi-based THHs.[15,30] From Fig. 2 it can be seen that the valence bands (VBs) and conduction bands (CBs) are weakly overlapped close to the Γ point of the Fermi level.

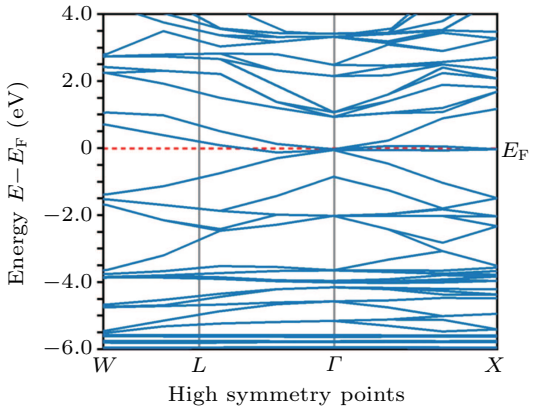


Fig. 2. Calculated band structure (BS) along high symmetry directions of ErPdBi.

This evidences the semi-metallic nature of the ErPdBi compound which is consistent with Ref. [11]. The bands (CBs and VBs) near the Fermi level are contributed mainly by the Pd-4d, 5s and Bi-6p, 6s states, due to degeneracy at the Γ point of ErPdBi indicating a non-trivial semimetal nature which is compatible with the previously reported study[11] and also consistent with the other THHs studies.[30]

3.2. Elastic properties and minimum thermal conductivity

Engineering applications of a given system require detailed investigation of the crystal elasticity, and three independent elastic constants of a cubic crystal is sufficient to describe the crystal elasticity according to the Voigt and Reuss schemes. The mechanical properties of a material such as stability, elastic moduli (B, G and Y), bonding nature, brittleness, ductility, hardness (H_V), machinability (μ_M), Poisson's ratio (ν), Pugh's ratio (B/G) and anisotropy can be narrated from the knowledge of elastic constants C_{ij}. These parameters have been calculated in this investigation at normal temperature and zero pressure, and summarized in Table 2. It can be seen that ErPdBi THH is a mechanically stable compound as the Born stability criteria are well satisfied (see Table 3): $C_{11}-C_{12}>0$, $C_{44}>0$ and $C_{11}+2C_{12}>0$.[31]

The bulk modulus (B) and shear modulus (G) measure the response of a solid material to the change of crystal volume and shape, respectively. On the other hand, Young's modulus (Y) measures the resistance against uniaxial tension. These basic parameters B, G and Y are usually large for a hard substances although they do not provide the information of hardnessas directly. Since the observed values of these parameters are comparatively large, the present study predicts larger hardness of THH ErPdBi (see Table 2). Another important elastic parameter is the elastic constant C_{11} that gives the hints of the elasticity along the length wise direction which can be useful for measuring the response to the stiffness of solid materials against the uniaxial strain. The large value of C_{11} indicates that ErPdBi is stiffer than the other half-Heuslers (LuPdBi and LaPdBi) belong to the same family.[15,17] The theoretical details of calculations of the above-mentioned parameters have been calculated using the following standard expressions:[17]

$$B = B_H = \frac{B_V + B_R}{2}, \tag{2}$$

$$G = G_H = \frac{G_V + G_R}{2}, \tag{3}$$

$$Y = \frac{9BG}{(3B+G)}, \tag{4}$$

$$\nu = \frac{(3B-2G)}{2(3B+G)}. \tag{5}$$

Table 2. The calculated elastic constants C_{ij} (in GPa), bulk modulus, B (in GPa), shear modulus G (in GPa), Young's modulus Y (in GPa), Pugh's indicator (B/G), machinability index μ_M, Poisson's ratio ν and Vicker's hardness H_V (in GPa) of ErPdBi ternary half-Heusler.

Compound	C_{11}	C_{12}	C_{44}	B	G	Y	B/G	μ_M	ν	H_V
ErPdBi	139.3	69.1	52.4	99.2	43.5	113.8	2.28	1.89	0.308	5.57

The relatively higher value of B for the THH ErPdBi indicates its high incompressibility compared to some isostructural other Bi-based THHs of LuPtBi, LuPdBi and LaPdBi.[14,15] At the same time, the resistance to plastic deformation can be measured by G and the calculated value of G in this study reflects the higher plastic deformation. Equally important, it is also revealed that the level of micro hardness is high for the ErPdBi system compared to the isostructural THH LuPdSb reported recently.[17]

The Pugh and Poisson's ratios can provide a useful link for brittle and ductile behaviors of solid necessary for practical applications. The Cauchy pressure is also a powerful tool for the prediction of brittle and ductile nature of solid materials. According to the limiting values of Pugh and Poisson's ratios mentioned in Refs. [31–33], it can be concluded that our material under study possesses ductile nature as the calculated values are 2.28 and 0.308, respectively. At the same time, a positive value of Cauchy pressure ($C_{12}-C_{44}$) indicates the ductile nature of a material. According to this scheme, the THH ErPdBi material should possess the ductile nature which has already been predicted by Pugh and Poisson's ratios.[34] Here, it should be noted that the interatomic force is basically central because of the value of Poisson's ratio is within the range 0.25–0.50.[35]

The calculated value of machinability index ($\mu_{\mathrm{M}} = \frac{B}{C_{44}}$)[36] of ErPdBi is larger (see Table 3) than LuPdBi (∼1.67, calculated using the given expression) and LuPdSb (∼1.70, calculated using the given expression) implies a good level of machinability than the other two THHs.[15,17] An empirical model used in Ref. [37] to calculate the hardness of materials can be expressed as $H_{\mathrm{V}} = \frac{(1-2\nu)Y}{6(1+\nu)}$, and the evaluated value is 5.57 GPa (see Table 2) for our system, which is fairly good for conventional applications.

For practical applications, the thermal conductivity is a very useful physical parameter, which can display the capability of heat conduction into the material. This parameter decreases with the increase of temperature T and towards a limiting value known as the minimum thermal conductivity κ_{min}. A lower value of the minimum thermal conductivity for efficient solid-state refrigeration is very important.[14] To improve the performance of optoelectronic devices as well as thermoelectric energy converters, the knowledge of minimum thermal conductivity is also important.[15] Considering the importance of this parameter, various methods have been introduced for the calculation of κ_{min}. Here, two familiar methods have been employed to describe the Cahill and Clarke models.[38,39]

Cahill models:

$$\kappa_{\mathrm{min}} = k_{\mathrm{B}} v_{\mathrm{m}} \left(\frac{N \rho N_{\mathrm{A}}}{M} \right)^{2/3}. \tag{6}$$

Clarke models:

$$\kappa_{\mathrm{min}} = 0.87 k_{\mathrm{B}} \left(M_{\mathrm{a}}\right)^{-2/3} Y^{1/2} \rho^{1/6}, \tag{7}$$

where $M_{\mathrm{a}} = \frac{M}{N_{\mathrm{A}} \times n}$.

It is noteworthy that the Clarke model is based on the density of materials whereas the Cahill model is based on the velocity of acoustic waves, which is associated with the lattice vibration. As the acoustic wave's velocity depends on the density of material significantly, both the methods are analogous, which has been discussed in Ref. [17]. It can also be noted that both the methods give reasonably close results (see Table 3). The crystal structure and the constituent atoms play a vital role in the exposure of lower minimum thermal conductivity, which can also be correlated with some significant thermophysical properties. The lower value of unit cell volume as well as the the larger mass of the atomic constituents results in larger density and this in turn is responsible for the manifestation of the low value of average sound velocity (v_{m}) and Debye temperature (Θ_{D}) of materials. We have found that the density of ErPdBi is high in comparison with the other listed materials in Table 3, and therefore it can be observed existence of comparatively lower average sound wave velocity (∼2221 m·s^{-1}) and Debye temperature Θ_{D} (∼199.80 K) along with low minimum thermal conductivity (0.453 from the Clarke model and 0.346 from the Cahill model) among other listed materials in Table 3.[17,38,40,41] An efficient way to enable the use of a compound in thermoelectric conversion is to reduce its thermal conductivity. There are also other concerns such as the construction of superlatives structures, molecular junctions, or the introduction of interfaces to prevent phonon transport.[42–46] However, in the present case, the studied compound is inherently low thermal conductive material. Therefore, it is expected that the compound ErPdBi should be suitable for use in thermoelectric conversion.

Table 3. Minimum thermal conductivity κ_{min} (in W·m^{-1}·K^{-1}) for ErPdBi.

Compound	κ_{min} Clarke	Reference	Compound	κ_{min} Clarke	κ_{min} Cahill	References
BeO	3.78	[38]	Ti_3AlN	1.198	1.410	[40]
SiC	3.00		$TiPt_3$	0.82	1.086	[41]
Al_2O_3	2.89		$ZrPt_3$	0.74	0.83	
MgO	2.56		$HfPt_3$	0.72	0.79	
AlN	2.45		LuPdSb	0.538	0.429	[17]
TiO_2	2.07		ErPdBi	0.453	0.346	our calculation

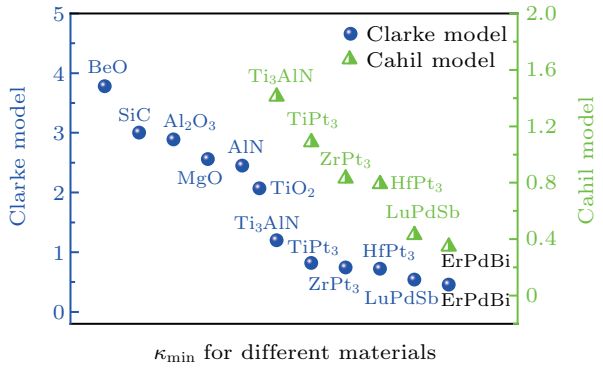


Fig. 3. The calculated κ_{min} of ErPdBi with available values of other materials.

We have observed that as listed in Table 3, the κ_{min} values of our studied material are comparatively lower than other species.[17,38,40,41] Figure 3 shows an interesting relation for different materials along with ErPdBi and displays the κ_{min} values. It can be clearly seen that our compound reveals the lowest value of κ_{min} compared to the compounds listed. Therefore, we may conclude that our studied material is more ideal in high-temperature applications. Thus the present study will encourage the future experimental research on the evaluation of minimum thermal conductivity for several purposes.

3.3. Anisotropy of elastic moduli, sound velocities and minimum thermal conductivity

Anisotropy is an engaging quantity in the crystal physics and engineering science, which clarifies the direction dependency of elastic properties of a material. In order to understand different properties such as behavior of micro-cracks in ceramics, development of plastic deformations into the crystals, propagation of cracks and to find mechanism to improve crystal durability as well as applications under different external environments, it is important to evaluate the elastic anisotropic factors in detail. The calculated elastic anisotropic factors have been listed in Table 4. The customarily used shear anisotropic indices in different directions for a cubic system (A_1, A_2, A_3) can be formulated by the following expressions.[47,48]

For $\langle 011\rangle$ and $\langle 010\rangle$ directions:

$$A_1 = \frac{4C_{44}}{C_{11}+C_{33}-2C_{13}}. \tag{8}$$

For $\langle 101\rangle$ and $\langle 001\rangle$ directions:

$$A_2 = \frac{4C_{55}}{C_{22}+C_{33}-2C_{23}}. \tag{9}$$

For $\langle 110\rangle$ and $\langle 010\rangle$ directions:

$$A_3 = \frac{4C_{66}}{C_{11}+C_{22}-2C_{12}}. \tag{10}$$

The estimated values of A_1, A_2, and A_3 showing moderate anisotropic behavior of ErPdBi (as all values are deviated from the unity). At the same time, all the factors are equal, which reflects the cubical symmetry of ErPdBi. Besides these shear anisotropy indices, there are some useful anisotropy indices. The elastic anisotropy of a material can also be manifested by the fractional anisotropy indices, namely fractional shear (A^G) and fractional bulk (A_B) anisotropy indices using the given expression:[47]

$$A^G = \frac{G_V - G_R}{2G_H}, \tag{11}$$

$$A_B = \frac{B_V - B_R}{B_V + B_R}. \tag{12}$$

From Table 4, A^G is higher than A_B ($A_B = 0$ as $B_H = B_R = B_V$), indicating that shear anisotropy of ErPdBi is larger than the anisotropy in compressibility. Moreover, to study the proper anisotropic nature we have also observed the universal anisotropic index A^U proposed by Ostoja–Shivakumar and Ranganathan as well as Zener anisotropy index (A), universal log-Euclidean index (A^L) and the equivalent Zener anisotropy (A^{eq}) using the following standard equations:[49–52]

$$A^U = 5\frac{G_V}{G_R} + \frac{B_V}{B_R} - 6 \geq 0, \tag{13}$$

$$A = \frac{2C_{44}}{C_{11}-C_{12}}, \tag{14}$$

$$A^L = \sqrt{\left[\ln\left(\frac{B^V}{B^R}\right)\right]^2 + 5\left[\ln\left(\frac{C_{44}^V}{C_{44}^R}\right)\right]^2}, \tag{15}$$

where

$$C_{44}^V = C_{44}^R + \frac{3}{5}\frac{(C_{11}-C_{12}-2C_{44})^2}{3(C_{11}-C_{12})+4C_{44}},$$

$$C_{44}^R = \frac{5}{3}\frac{C_{44}(C_{11}-C_{12})}{3(C_{11}-C_{12})+4C_{44}},$$

$$A^{eq} = \left(1+\frac{5}{12}A^U\right) + \sqrt{\left(1+\frac{5}{12}A^U\right)^2 - 1}. \tag{16}$$

The factor A^U is termed as universal due to its applicability to all sorts of crystal symmetries. The calculated value (see Table 4) of the universal anisotropy index indicates the anisotropic nature of ErPdBi as predicted previously by fractional anisotropy and shear anisotropy indices. Another anisotropy index is universal log-Euclidean index (A^L). The condition for isotropic crystal is $A^L = 0$. The positive value A^L and the deviation from zero indicate the perfect anisotropic nature of a solid. On the other hand, about 90% compounds have $A^L < 1$ but a very few materials belong to the range from 0 to 10.26. It is worth mentioning that A^L is also an indicator of the layered/lamellar type of configuration.[52] On the contrary, a higher value of A^L shows strong layered structural features, whereas a lower A^L implies non-layered structure. It can be seen that A^L possesses a lower value (see Table 4) that exhibits moderately layered configuration of ErPdBi. It is well known that for an isotropic crystal, A^{eq} is unity. Therefore, the calculated value of A^{eq} is 1.489, predicted that our studied material is anisotropic in nature.

Table 4. Calculated shear anisotropic factors (A_1, A_2 and A_3), Zener's anisotropy index (A), Anisotropy in shear (A^{G}), anisotropy in bulk modulus (A_{B}), universal log-Euclidean index (A^{L}), universal anisotropy index (A^{U}) and equivalent Zener anisotropy measure (A^{eq}) of the ErPdBi cubic system.

Compound	A_1	A_2	A_3	A	A^{G}	A_{B}	A^{L}	A^{U}	A^{eq}
ErPdBi	1.49	1.49	1.49	1.49	0.038	0	0.323	0.193	1.489

To estimate and to visualize the direction dependency of ErPdBi, we have also depicted 3D graphical representation of Young's modulus (Y), shear modulus (G), and Poisson's ratio (v) (see Fig. 4). It is clearly seen that the present study showing the anisotropic nature in all planes along all directions of ErPdBi system. In addition, we have also listed the minimum and maximum limits of Y, G and v in Table 5, from which it can be observed that the anisotropy increases in the order of $Y < G < v$.

Table 5. The minimum and maximum limits of Y (in GPa), G (in GPa) and v for the ErPdBi cubic system.

Compound	Young's modulus		Shear modulus		Poisson's ratio	
ErPdBi	$Y_{\min}$	$Y_{\max}$	$G_{\min}$	$G_{\max}$	$v_{\min}$	$v_{\max}$
	90.55	132.11	33.89	52.40	0.131	0.439

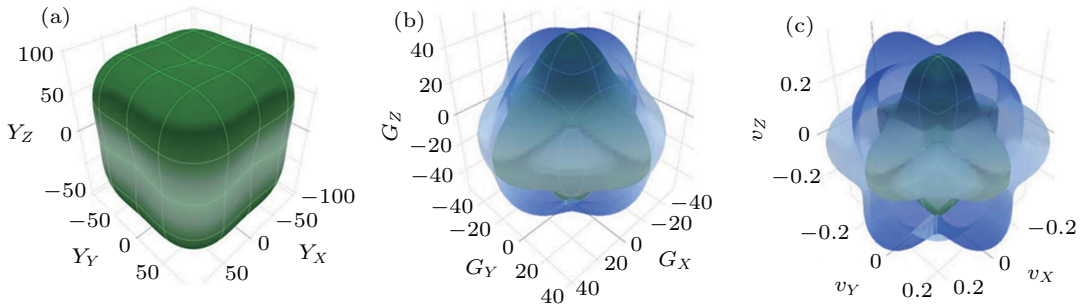


Fig. 4. Directional dependency (anisotropy) in (a) Young's modulus, Y (in GPa), (b) shear modulus, G (in GPa) and (c) Poisson's ratio, ν of ErPdBi cubic ternary half-Heusler.

Furthermore, to understand the lattice dynamical anisotropy in ErPdBi, it is imperious to calculate acoustics velocities in various propagation directions. Due to the cubic nature of our studied material, we have applied Brugger's suggested methods[53] to evaluate the sound velocities in different directions, as listed in Table 6. The different acoustics velocities along [111], [110] and [100] directions can be expressed as[54]

$$
\begin{aligned}
&[100]\, v_{\mathrm{l}} = \sqrt{\frac{C_{11}}{\rho}}, \quad [010]\, v_{\mathrm{t1}} = [001]\, v_{\mathrm{t2}} = \sqrt{\frac{C_{44}}{\rho}},\\
&[110]\, v_{\mathrm{l}} = \sqrt{\frac{(C_{11}+C_{12}+2C_{44})}{2\rho}},\\
&[1\bar{1}0]\, v_{\mathrm{t1}} = \sqrt{\frac{(C_{11}-C_{12})}{\rho}},\\
&[001]\, v_{\mathrm{t2}} = \sqrt{\frac{C_{44}}{\rho}}, \quad [111]\, v_{\mathrm{l}} = \sqrt{\frac{(C_{11}+2C_{12}+4C_{44})}{3\rho}},\\
&[11\bar{2}]\, v_{\mathrm{t1}} = v_{\mathrm{t2}} = \sqrt{\frac{(C_{11}-C_{12}+C_{44})}{3\rho}}. \qquad (17)
\end{aligned}
$$

In addition, the heat is transmitted through solid materials in three different modes: by the movement of free electrons in metals, by the thermal vibrations of atoms and by radiation (if they are transparent). Among them, transmission by thermal vibrations indicates the propagation of elastic waves. One can easily find that an elastically anisotropic solid has anisotropic minimum thermal conductivity ($\kappa_{\min}$). Therefore, the anisotropic nature of minimum thermal conductivity depends on acoustics velocity in different crystallographic directions. The factor $\kappa_{\min}$ along different directions is evaluated by using Clarke and Cahill model:[39]

$$\kappa_{\min} = \frac{k_{\mathrm{B}}}{2.48} n^{2/3} (v_{\mathrm{l}} + v_{\mathrm{t1}} + v_{\mathrm{t2}}), \qquad (18)$$

where $n = N/V$.

Table 6. Anisotropic sound velocities (in m·s^{-1}) of ErPdBi along different crystallographic directions.

Anisotropic sound velocities		ErPdBi
[111]	$[111]v_{\mathrm{l}}$	3838.71
	$[11\bar{2}]\, v_{\mathrm{t1,2}}$	1925.85
[110]	$[110]v_{\mathrm{l}}$	3769.92
	$[1\bar{1}0]\, v_{\mathrm{t1}}$	2524.09
	$[001]v_{\mathrm{t2}}$	2180.74
[100]	$[100]v_{\mathrm{l}}$	3555.59
	$[010]v_{\mathrm{t1}}$	2180.74
	$[001]v_{\mathrm{t2}}$	2180.74

In the above equation, k_{B} is the Boltzmann constant, n defines the number of atoms per unit volume, and N is defined by the total number of atoms in the cell having a volume V.

Table 7. The number of atom per mole of the compound n (m^{-3}), minimum thermal conductivity (W/m·K) of the ErPdBi compound along different directions.

Compound	n	$\kappa_{\min}$		
		$[111]\kappa_{\min}$	$[110]\kappa_{\min}$	$[100]\kappa_{\min}$
ErPdBi	4.134×10^{28}	0.512	0.563	0.526

The minimum thermal conductivity of ErPdBi along [111], [110] and [100] directions are listed in Table 7. We can conclude that the minimum thermal conductivities are

higher along with different crystallographic directions than the isotropic minimum thermal conductivity of the material under study (see Subsection 3.2).

3.4. Optical properties

To understand the response of a material to incident electromagnetic radiation (e.m.), it is necessary to study the various optical properties of the material as a function of photon energy, E (eV). Therefore, calculations of these properties in detail are covetable in order to search the potential application of materials in a wide range of optoelectronic devices. In this point of view, we have calculated different optical parameters of ErPdBi for the incident photon energies up to 15 eV, where the field polarization vectors have been only considered in the direction [001] as for cubic phase $\varepsilon_{xx} = \varepsilon_{yy} = \varepsilon_{zz}$.[55] On the other hand, due to the semi-metallic nature of our studied compound,[11] we have used an unscreened plasma frequency of 5 eV and damping of 0.05 eV[56] to begin the calculation of the optical constants of the ErPdBi THH material. The value of Gaussian smearing is set to 0.5 eV so that k-points mesh becomes more effective in the Fermi surface. The real and imaginary parts of dielectric function have been presented in Fig. 5(a). As is seen from Fig. 5(a), both the real and imaginary parts of dielectric function are high in low frequency region and starts to fall with the increase of the energy of the incident photon. This nature of dielectric curve is important for the microelectronics device applications and large scale integration of integrated circuits.[15,57] Both the spectra have a broad minor peaks in between 0 to 5 eV, which is because of dominant intra band transition for the semi metallic nature of ErPdBi.[15] At the same time, ErPdBi has dielectric response even at zero incident photon energy, which is commonly known as static dielectric constant and has a larger value approximately equal to 80. This large value of dielectric constant at zero frequency suggestive to the applicability of our material for dielectric purposes under zero photon energy.

Among the optical parameters, another complex parameter is the refractive index $N(\omega)$ that is the sum of real part $n(\omega)$, which comprises the phase velocity and imaginary part $k(\omega)$, which represents the loss of e.m. wave when it travels through a solid. The refractive index, which has both real and imaginary parts, is depicted in Fig. 5(b) for ErPdBi. The transition of an electron between the valence band (VB) and conduction band (CB), i.e., VB→CB, which results in the peak in the refractive index spectra. The real part falls gradually with a similar fashion depicted in the case of real part of the dielectric function, on the other hand, imaginary part exceeds the real part nearly at 4.5 eV and starts to increase up to 6 eV and then again falls down below real part nearly at 13 eV. The maximum peak of refractive index (∼10) is obtained at zero photon, which suggests that the studied material has potential applications in the device applications such as QLED, OLED, solar cell and waveguides.[56,58]

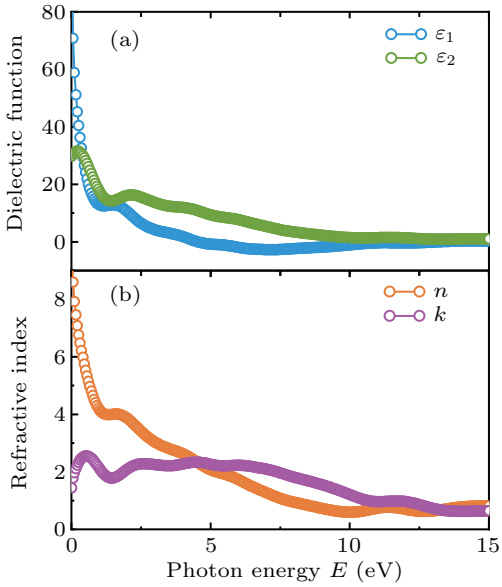


Fig. 5. Calculated (a) dielectric function (real and imaginary) and (b) refractive index (real and imaginary) as a function of incident photon energy E (eV) along [001] polarization direction.

Optical conductivity spectra are much important for the characterization of material in display device applications which arise due to the incident photons of suitable energy. It results in increase the number of electrons in CB and holes within VB. The electrical conductivity (photoconductivity) of the material increases with increasing photon energy and the spectra attain its maximum value in the spectral region from ∼2.5–6.2 eV energy (see Fig. 6(a)). Thus, the material is expected or be extremely electrically conductive, which ensures the conventional application sides of this compound under study.

To understand the conversion of optimum photon energy (solar energy) into the efficiency of a material, the absorption co-efficient is a necessary factor that enlightens the decomposition of light intensity covering in a unit distance. The optical absorption coefficient may onset is due to the free electrons within the CB of materials. This coefficient offers the knowledge on the light harvesting capability of a material, which can enable us to explain the efficiency of solar cells as a function of incident energy. The absorption coefficient is quite high at energy ∼5.15–8.36 eV, which ensures the potential application in solar panels. Hence, it is observed in Fig. 6(b) that the absorption spectra start at zero energy, and ErPdBi has no band gap, which can also be confirmed from band structure calculation (see Subsection 3.1).

Figure 7(a) exhibits the reflectivity spectra of the ErPdBi compound. It is seen that the reflectivity values of the studied compound are significantly low in the low energy region. We have observed that the reflectance is interestingly low in the IR-visible region (∼0.00–3.26 eV), which suggests that if

this material is used in the solar panel, it will allow necessary visible spectra for producing photocurrent, and this, in turn, will raise the efficiency of solar panels greatly. On the other hand, the high value of reflectance (∼48%) at 7.50–9.35 eV photon energy proves the superiority of ErPdBi for promising to reduce solar heating.

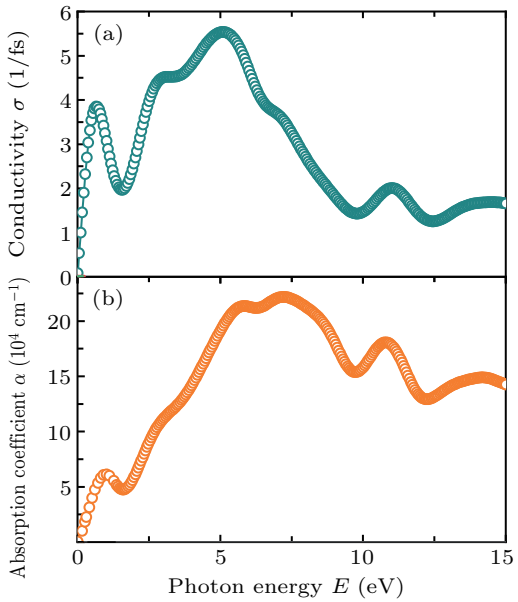


Fig. 6. Calculated (a) conductivity and (b) absorption coefficient versus incident photon energy E (eV) along [001] polarization direction.

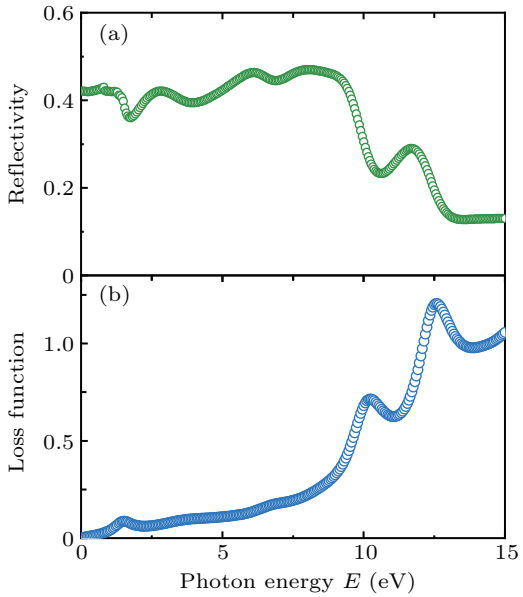


Fig. 7. Calculated (a) reflectivity and (b) energy loss function as a function of incident photon energy E (eV) along [001] polarization direction.

The frequency-dependent electron energy-loss function is depicted in Fig. 7(b). At a particular incident photon frequency, a large peak is observed in $L(\omega)$ spectra–known as the plasma frequency, ω_P (screened). To do so, the studied material will be transparent and will switch from its metallic to dielectric response when the incident photon has a greater energy than the plasma frequency.

4. Conclusion

In summary, we have investigated the elastic, optical and anisotropic properties of ErPdBi successfully using DFT tools. This is the first detailed study of these properties for the titled compound. The calculated cell parameter and unit cell volume are in agreement well with the available theoretical and experimental data. Elastic investigation reveals that ErPdBi is a mechanically stable compound and possesses ductile nature. On the other hand, the observed minimum thermal conductivity calculated in two different methods reveals that the value of minimum thermal conductivity for ErPdBi is very low compared to the others species. Therefore, the material under study can be applied for high temperature thermal barrier coating. We have observed that ErPdBi is highly anisotropic in elastic moduli, acoustic velocities and even in minimum thermal conductivity despite its cubic structure. Judging from the dielectric function, refractive index and reflectivity spectra it can be concluded that our material has a great potential in a wide range of optoelectronic device applications, such as microelectronics, ultra-large-scale integration of integrated circuits, OLED, solar cells (increasing photocurrent), waveguides and reducing solar heating as well.

Author contributions

R. Majumder: Conceptualization, formal analysis, supervision, writing-original draft, writing-review & editing. S. K. Mitro: supervision, methodology, formal analysis, investigation, writing-original draft, writing-review & editing. K. M. Hossain: formal analysis, validation, writing-review & editing. Md. Zahid Hasan: formal analysis, writing-review & editing. Md. Emran Hossain: formal analysis, writing-review & editing. M. A. Hadi: formal analysis, writing-review & editing.

Data availability

All data needed to evaluate the conclusion of this study are presented in the paper. Additional data are available from the corresponding author upon reasonable request.

References

[1] Dhar S K, Nambudripad N and Vijayaraghavan R 1988 *J. Phys. F* **18** L41
[2] Pierre J and Karla I 2000 *J. Magn. Magn. Mater.* **217** 74
[3] Bay T V 2014 *Solid State Commun.* **183** 13
[4] Jung M H, Yoshino T, Kawasaki S, Pietrus T, Bando Y, Suemitsu T, Sera M and Takabatake T 2001 *J. Appl. Phys.* **89** 7631
[5] Bhattacharya S, Pope A L, Littleton IV R T, Tritt T M, Ponnambalam V, Xia Y and Poon S J 2000 *Appl. Phys. Lett.* **77** 16
[6] Barman C K and Alam A 2018 *Phys. Rev. B* **97** 075302
[7] Shekhar C, Ouardi S, Nayak A K, Fecher G H, Schnelle W and Felser C 2012 *Phys. Rev. B* **86** 155314
[8] Mukhopadhyay A, Mahana S, Chowki S, Topwal D and Mohapatra N 2017 *AIP Conf. Proc.* **1832** 110024
[9] Winiarski M J and Bilinska K 2019 *Intermetallics* **108** 55
[10] Pavlosiuk O, Filar K, Wisniewski P and Kaczorowski D 2015 *Acta Phys. Pol. A* **127** 656

[11] Pan Y, Nikitin A M, Bay T V, Huang Y K, Paulsen C, Yan B H and de Visser A 2013 *Europhys. Lett.* **104** 27001
[12] Sekimoto T, Kurosaki K, Muta H and Yamanaka S 2006 *J. App. Phys.* **99** 103701
[13] Pavlosiuk O, Fabreges X, Gukasov A, Meven M, Kaczorowski D and Wiśniewski P 2018 *Physica B* **536** 56
[14] Majumder R and Hossain M M 2019 *Comput. Condens. Matter* **21** e00402
[15] Majumder R, Hossain M M and Shen D 2019 *Mod. Phys. Lett. B* **33** 1950378
[16] Gruhn T 2010 *Phys. Rev. B* **82** 125210
[17] Majumder R, Mitro S K and Bairagi B 2020 *J. Alloys Compd.* **836** 155395
[18] Clark S J, Segall M D, Pickard C J, Hasnip P J, Probert M I J, Refson K and Payne M C 2005 *Z. Kristallogr.* **220** 567
[19] Hohenberg P and Kohn W 1964 *Phys. Rev.* **136** B864
[20] Kohn W and Sham L J 1965 *Phys. Rev.* **140** A1133
[21] Perdew J P, Burke K and Ernzerhof M 1996 *Phys. Rev. Lett.* **77** 3865
[22] Vanderbilt D 1990 *Phys. Rev. B* **41** 7892
[23] Majumder R and Mitro S K 2020 *RSC Adv.* **10** 37482
[24] Monkhorst H J and Pack J D 1976 *Phys. Rev. B* **13** 5188
[25] Fischer T H and Almlof J 1992 *J. Phys. Chem.* **96** 9768
[26] Nielsen O H and Martin R M 1983 *Phys. Rev. Lett.* **50** 697
[27] Saha S, Sinha T P and Mookerjee A 2000 *Phys. Rev. B* **62** 8828
[28] Tse G and Yu D 2015 *Comput. Condens. Matter* **4** 59
[29] Huang S, Liu X, Zheng W, Guo J, Xiong R, Wang Z and Shi J 2018 *J. Mater. Chem. A* **6** 20069
[30] Shrivastava D and Sanyal S P 2018 *Physica C* **544** 22
[31] Shekhar C, Ouardi S, Nayak A K, Fecher G H, Schnelle W and Felser C 2012 *Phys. Rev. B* **86** 155314
[32] Pugh S F 1954 *Lond. Edinb. Dubl. Phil. Mag. J. Sci.* **45** 823
[33] Fu H, Li D, Peng F, Gao T and Cheng X 2008 *Comput. Mater. Sci.* **44** 774
[34] Pettifor D G 1992 *Mater. Sci. Technol.* **8** 345
[35] Rubel M H K, Mitro S K, Mondal B K, Rahaman M M, Saiduzzaman M, Hossain J and Kumada N 2020 *Physica C* **574** 1353669
[36] Chen X Q, Niu H and Li D, Li Y 2011 *Intermetallics* **19** 1275
[37] Mattesini M, Ahuja R and Johansson B 2003 *Phys. Rev. B* **68** 184108
[38] Clarke D R 2003 *Surf. Coat. Technol.* **163** 67
[39] Cahill D G, Watson S K and Pohl R O 1992 *Phys. Rev. B* **46** 6131
[40] Wang J *et al.* 2014 *J. Solid State Chem.* **216** 1
[41] Mitro S K, Rahman M A, Parvin F and Islam A K M A 2019 *Int. J. Mod. Phys. B* **33** 1950189
[42] Chen X K, Xie Z X, Zhou W X, Tang L M and Chen K Q 2016 *Appl. Phys. Lett.* **109** 023101
[43] Zeng Y Z, Wu D, Cao X H, Zhou W X, Tang L M and Chen K Q 2020 *Adv. Funct. Mater.* **30** 1903873
[44] Zhou W X, Cheng Y, Chen K Q, Xie G F, Wang T and Zhang G 2020 *Adv. Funct. Mater.* **30** 1903829
[45] Wu D, Cao X H, Jia P Z, Zeng Y J, Feng Y X, Tang L M, Zhou W X and Chen K Q 2020 *Sci. Chin.-Phys. Mech. Astron.* **63** 276811
[46] Chen X K and Chen K Q 2020 *J. Phys.: Condens. Matter* **32** 153002
[47] Gao X P, Jiang Y H, Zhou R and Feng J 2014 *J. Alloys Compd.* **587** 819
[48] Ravindran P, Fast L, Korzhavyi P A and Johansson B 1998 *J. Appl. Phys.* **84** 4891
[49] Chung D H and Buessem W R 1967 *J. Appl. Phys.* **38** 2010
[50] Gueddouh A, Bentria B and Lefkaier I 2016 *J. Magn. Magn. Mater.* **406** 192
[51] Kube C M 2016 *AIP Adv.* **6** 095209
[52] Kube C M and Jong M D 2016 *J. Appl. Phys.* **120** 165105
[53] Brugger K 1965 *J. Appl. Phys.* **36** 768
[54] Duan Y H, Sun Y, Peng M J and Zhou S G 2014 *J. Alloys Compd.* **595** 14
[55] Rahman M A, Mitro S K, Parvin F and Islam A K M A 2020 *Indian J. Phys.* (in press)
[56] Naher M I and Naqib S H 2020 *J. Alloys Compd.* **829** 154509
[57] Majumder R, Sarker M A R, Hossain M M, Hossain M E, Shen D, Reza A K M S and Kabir M H 2019 *J. Sci. Res.* **11** 195
[58] Rubel M H K, Hossain K M, Mitro S K, Rahman M M, Hadi M A and Islam A K M A 2020 *Mater. Today Commun.* **24** 100935